Preparation of TiO_2@ZIF-8 for the removal of As(III) in water

Guangpeng Li, Hui Jiang, Dan Li, Tianyu Liao, Lingling Yuan and Wenhua Geng

ABSTRACT

To remove As(III) in water, the composite material of TiO_2@ZIF-8 was prepared by a sol-gel method with zeolitic imidazolate framework-8 (ZIF-8) as the matrix. The structure of TiO_2@ZIF-8 was characterized with scanning electron microscopy (SEM), X-ray powder diffraction (XRD), and Fourier transform infrared spectroscopy (FT-IR). The results indicated that the best loading efficiency of TiO_2 on ZIF-8 occurred when it was calcined at 300 °C for 3 h. This material was used to remove As(III) from aqueous solution, and the effect of the initial concentration of As(III), pH, and the illumination condition on the removal of As(III) was investigated. The results showed that the removal rate of As(III) was as high as 100% under a pH of 4–7, an initial As(III) concentration of less than 2 mg/L, and UV-light irradiation for 2 h. The repeated experiments were also performed for the investigation of the stability of TiO_2@ZIF-8.

Key words | As(III), composite material, removal rate, TiO_2@ZIF-8

Guangpeng Li
Hui Jiang
Dan Li
Tianyu Liao
Lingling Yuan
Wenhua Geng (corresponding author)
College of Biotechnology and Pharmaceutical Engineering,
Nanjing Tech University,
Nanjing 211816,
China
E-mail: *gengwenhua@njtech.edu.cn*

INTRODUCTION

Due to the development of mining industries and the exclusive use of arsenical pesticides, the area of arsenic contamination is rising in developing countries (Mohan & Pittman 2007). So for people living in this area, long-term exposure to arsenic, even ingestion of contaminated water, will lead to diseases like skin lesions and cancers of the brain, liver, kidney, and stomach. Therefore, the maximum contaminant level of arsenic in drinking water was recommended by the World Health Organization (WHO) to be 10 μg/L in 1993. Arsenic contamination in water is mainly caused by nonionic trivalent (As(III)) and ionic pentavalent (As(V)) arsenic, and the different proportions of As(III) and As(V) depend on the environmental conditions of the aquifer, such as redox conditions, pH, biological activity, and adsorption reactions. The toxicity of As(III) is over 60 times greater than that of As(V), and, in addition, As(III) is more difficult to remove from water by most techniques (Zhang *et al.* 2017). At present, the mainstream technology of removal of As(III) from water is peroxidation to As(V) by an oxidant and adsorption of the As(V). Among different oxidation treatments (such as ozone, hydrogen peroxide, potassium ferrate, and photocatalytic oxidation), photocatalytic oxidation has been proven to be a useful approach in oxidizing As(III) to As(V) (Guan *et al.* 2012). Among all photocatalysts, titanium dioxide (TiO_2), the most common semiconductor photocatalyst, is a promising material for removing arsenic, especially As(III) (Bissen *et al.* 2001; Pirila *et al.* 2011).

Photocatalysis with TiO_2 offers a relatively inexpensive, environmentally benign way to achieve As(III) oxidation. Moreover, TiO_2 can also work as an adsorbent to remove arsenic from water. The bi-functional property of TiO_2 gives it an additional advantage, and many studies have been carried out to investigate arsenic removal by TiO_2 (Bang *et al.* 2005). However, the low adsorption capacity and the problem of separating TiO_2 powder from an

doi: 10.2166/ws.2017.074

aqueous solution usually limit its application in arsenic removal (Qu 2008). Furthermore, the direct application of suspended TiO_2 powders in drinking water treatment may be problematic due to the difficulty of separation and recovery of the tiny particles. In order to overcome this drawback and combine the advantages of TiO_2, the supported TiO_2 is becoming a better choice for the field application of the photocatalyst. As is usual, the support material has the properties of high surface area, absorption capacity, and chemical stability. Compared with conventional adsorbents (such as activated carbon, activated alumina, and zeolite), zeolitic imidazolate framework-8 (ZIF-8) has a higher surface area and adsorption activity (Liu *et al.* 2015).

ZIF-8, formed by imidazole ligands and metal ions, is a kind of metal-organic framework, and has potential selectivity in adsorption, gas separation, and capturing target materials, etc. ZIF-8 has perfect adsorption ability for As(V), but has a very low adsorption affinity for As(III) as it is a neutral molecular species in a large pH range. Jian *et al.* (2015) used ZIF-8 to adsorb As(V) up to 99.94%, in contrast the adsorption rate of As(III) was only 27% under ZIF-8 dosage of 0.2 g/L for 100 μg/L As(III) or As(V). Considering the adsorption ability of ZIF-8 for As(V) and the oxidation capacity of TiO_2 for As(III), we have a proposition to synthesize the composite material of TiO_2@ZIF-8 for removal of As(III). In recent years, TiO_2 and adsorbent heterostructures have been reported for removal of As(III) in water, such as TiO_2-activated carbon (Liu *et al.* 2014), magnetic Fe_3O_4@TiO_2 (Lan 2015), and TiO_2-chitin (Miller & Zimmerman 2010). Moreover, photocatalysts loaded on the surface of ZIF-8 were also reported for degradation of organic dye, such as ZnO@ZIF-8 and TiO_2@ZIF-8 (Chandra *et al.* 2015; Yu *et al.* 2015).

To the best of our knowledge, no one has ever reported the removal of As(III) by TiO_2@ZIF-8, and the concentration of arsenic in drinking water is generally less than 500 μg/L, even in the two worst affected areas, Bangladesh and West Bengal, India (Mazumder *et al.* 1998). Furthermore, the pH of drinking water is close to neutral, so we chose TiO_2@ZIF-8 to deal with the low concentration of As(III) in water at neutral conditions. In this paper, the composite material of TiO_2@ZIF-8 was synthesised, and its properties were investigated. Then the adsorption kinetic and isotherm of TiO_2@ZIF-8 for As(III) were conducted under protection from light. Finally, we carried out an experiment to remove As(III) from aqueous solution, and discussed the effect on As(III) removal of the different factors.

MATERIALS AND METHODS

Chemicals and materials

Analytical grade chemicals were used without any further purification. Tetrabutyltitanate $Ti(OBu)_4$ was purchased from Shanghai Zhanyun Chemical Co., Ltd (Shanghai, China); 2-methylimidazole was obtained from Shanghai Baiao Biological Technology Co., Ltd (Shanghai, China); and $Zn(NO_3)_2{\cdot}6H_2O$ was purchased from Xilong Chemical Co., Ltd (Guangdong, China). A standard solution of 1,000 mg/L As (III) was purchased from O2si smart solutions (Charleston, SC, USA), and this was diluted just before use. All volumetric flasks and vessels were soaked in 10% HNO_3 for at least 24 h, and then rinsed for several times with ultra-pure water from a Sartorius water purification system (Mini plus, Sartorius, Germany).

Preparation of ZIF-8 nanoparticles and TiO_2@ZIF-8 materials

ZIF-8 nanoparticles were synthesized by a liquid phase diffusion method. In a typical synthesis, 1.5 g $Zn(NO_3)_2{\cdot}6H_2O$ and 3.3 g 2-methylimidazole were dissolved in 70 mL anhydrous methanol. Then the solution of 2-methylimidazole was slowly added to another solution under stirring at room temperature (25 ± 2 °C). After stirring for 24 h, the product was collected by centrifugation at 8,000 rpm for 10 min, and then washed with anhydrous methanol three times. The obtained ZIF-8 nanoparticles were dried in a vacuum drying oven at 110 °C for 24 h to remove residual methanol, and kept in a desiccator before use.

TiO_2@ZIF-8 was prepared by a sol-gel method at room temperature using $Ti(OBu)_4$ as the precursor. First, 0.6 mL acetic acid was added to 10 mL absolute alcohol as a stabilizer of the solution, and then 4 mL $Ti(OBu)_4$ and 10 g ZIF-8 were added to the solution and mixed well by a magnetic stirrer for 2 h. Next, 0.6 mL acetic acid and 1.6 mL

ultra-pure water were added to 5 mL absolute alcohol, and the pH was adjusted by concentrated nitric acid to 3 under vigorous stirring. Then the second solution was slowly added to the first solution at room temperature followed by stirring for 4 h. The titanium sol/ZIF-8 turned into titanium gel/ZIF-8 after aging for 24 h at 25 °C, and it was then dried at 60 °C. The powder was calcined at different temperatures ranging from 100 °C to 400 °C for 3 h. The obtained composite materials were kept in a desiccator before use.

Characterization

The morphologies of TiO_2@ZIF-8 and ZIF-8 were examined by a scanning electron microscope (SEM, Ultra-55, Carl Zeiss, Germany). X-ray powder diffraction (XRD, D/max-r B, Rigaku Corporation, Japan) analysis was carried out on a diffractometer with Cu-Kα target (40 kV, 100 mA, $\lambda =$ 1.5418 Å) from 5° to 80°. The functional groups on the TiO_2-@ZIF-8 were identified at room temperature by Fourier transform infrared spectroscopy (FT-IR, Nicolet 6700, Thermo Fisher, USA). All samples were dried for 24 h at 60 °C prior to the KBr preparation in order to avoid water related bands interference.

Removal of As(III)

The experiments on As(III) removal were carried out using a xenon lamp (300 W) as the irradiation source at room temperature. An initial As(III) concentration of 2 mg/L and a pH of 7.0 ± 0.1 were used in most experiments, while the amount of TiO_2@ZIF-8 powder was 0.04 g/L. The suspension of As(III)-TiO_2@ZIF-8 was in the dark for 1.5 h to allow adsorption equilibrium before it was illuminated by UV-light ($\lambda < 400$ nm) or visible light ($\lambda > 400$ nm). Samples of the suspension were withdrawn after 30 min intervals and filtered through a 0.22 μm membrane. The filtrates were analyzed for the residual concentration of the different species of arsenic, especially As(III) and As(V). To compare the removal efficiency of As(III) by TiO_2@ZIF-8, the pure TiO_2 and ZIF-8 were tested. Additionally, the effect of the media pH, the initial concentration of As(III), the interaction time, and the illumination condition were also determined. Adsorption isotherm experiments of As(III) on TiO_2@ZIF-8 were conducted in dark conditions, and with the initial concentration of As(III) ranging from 0.2 mg/L to 10 mg/L, pH 7.0 ± 0.1, solid/solution ratio of 0.04 g/L, and stirring for 5 h at 25 ± 1 °C. Furthermore, the adsorption kinetics of As(III) by TiO_2, ZIF-8, and TiO_2@ZIF-8 were also tested in dark conditions.

To detect the different species of arsenic in samples, an atomic fluorescence spectrometer coupled with liquid chromatography (LC-AFS, LC-AFS 9600, Beijing Haiguang instrument, China) was used, which was equipped with a Hamilton PRP-X100 anion-exchange column (250 mm × 4.1 mm). The mobile phase was a pH 5.6 phosphate buffer prepared with 2.26 g $Na_2HPO_4 \cdot 12H_2O$ and 3.03 g KH_2PO_4 with ultra-pure water to 500 mL. The reducing solution was a mixture of 5 g/L NaOH and 10 g/L KBH_4, with 5% (v/v) hydrochloric acid as the carrier solution.

The recycling method of TiO_2@ZIF-8 was as follows: the TiO_2@ZIF-8 that had been used for the removal of As(III) was filtered, desorbed using 0.1 mol/L NaOH under stirring for 24 h, and then washed with ultra-pure water three times, and finally dried in a vacuum drying oven at 110 °C for 24 h.

RESULTS AND DISCUSSION

Characterization of TiO_2@ZIF-8

Calcination is a common treatment used to improve the crystallinity of TiO_2 powders, and the XRD patterns of TiO_2@ZIF-8 calcined at the different temperatures are shown in Figure 1. We found that the strength of the characteristic peaks of TiO_2 increased with the rise in calcination temperature when the calcination temperature ranged from 100 °C to 300 °C. However, when the calcination temperature was up to 400 °C, the TiO_2@ZIF-8 was amorphous, because the thermo-stability of ZIF-8 is about 350 °C, which was in agreement with previous reports (Tran *et al.* 2011). The XRD patterns of TiO_2@ZIF-8 calcined at 300 °C and ZIF-8 are shown in Figure 2, and the TiO_2@ZIF-8 was composed of a TiO_2/ZIF-8 hybrid structure: the peaks at 2θ values of 25.3°, 37.9°, 48.1°, 54.16°, 55.32°, and 62.7° could be indexed to the (101), (004), (200), (105), (211), and (204) crystal planes of TiO_2, respectively (Wei *et al.* 2016). The peaks at 7.26°, 10.32°, 12.64°, 17.96°, and 26.62° corresponded to the (011), (002), (112), (222), and (134) of

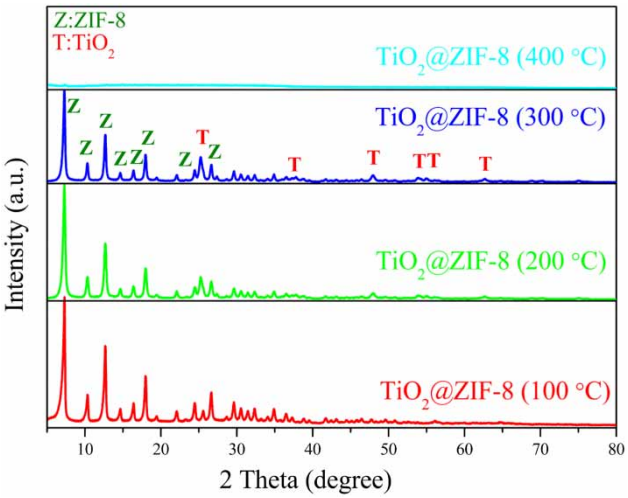

Figure 1 | XRD patterns of TiO_2@ZIF-8 at the different calcination temperatures. The diffraction peaks of the TiO_2 phase are marked with T, and the diffraction peaks of the ZIF-8 phase are marked with Z.

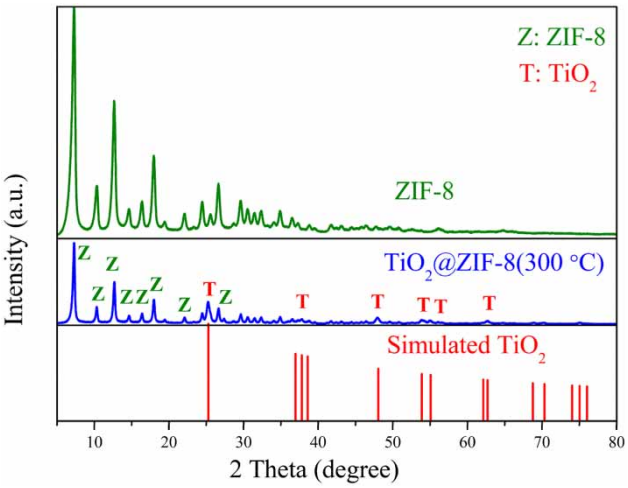

Figure 2 | XRD patterns of TiO_2@ZIF-8 calcined at 300 °C, ZIF-8, and simulated TiO_2 (PDF21-1272).

the structure of ZIF-8, respectively (Zhu *et al.* 2011). Both the characteristic peaks of TiO_2 and ZIF-8 were found in TiO_2@ZIF-8, which indicated the combination of ZIF-8 and TiO_2. The peak strength of TiO_2 was weaker than that of ZIF-8, which may be caused by the lower content of TiO_2 than ZIF-8 in the composite material, because the molar ratio of Zn to Ti was about 16.8:1. On the other hand, the peak strength of ZIF-8 in the composite material was weaker than the ZIF-8 nanoparticle, which may be attributed to the effect of calcination.

In Figure 3, the SEM micrographs of TiO_2@ZIF-8 calcined at the different temperatures and the original ZIF-8 are shown. From Figure 3 and combined with the analytic results of XRD (Figure 1), the larger particles of the precursor of TiO_2 but not TiO_2 were found to densely adhere to the surface of ZIF-8 when the calcination temperature was 100 °C. When the calcination temperature was elevated to 300 °C, the precursor of TiO_2 could hardly be seen, and TiO_2 clearly adhered to the surface of ZIF-8. However, when the calcination temperature was up to 400 °C, the pore structure of the ZIF-8 had been damaged (Tran *et al.* 2011), and the large amount of TiO_2 that adhered to the surface of ZIF-8 had been dropped. From the above observations, the crystallinity of TiO_2 increased while the crystallinity of ZIF-8 decreased as the calcination temperature increased in the range from 100 °C to 300 °C, so we may come to the conclusion that the best calcination temperature is 300 °C, and TiO_2@ZIF-8 calcined at 300 °C was used in the following experiments.

The FT-IR spectra of TiO_2@ZIF-8 calcined at 300 °C and ZIF-8 nanoparticles in the range of 2,000–400 cm^{-1} are plotted in Figure 4. The FT-IR analysis of TiO_2@ZIF-8 revealed the presence of an adsorption band at 420 cm^{-1} (Zn-N stretch), another adsorption band at 1,584 cm^{-1} (C = N stretch), and also two bands at 996 cm^{-1} and 1,425 cm^{-1} (C-N stretch), which were typically characteristic for ZIF-8 (Hu *et al.* 2011). The absorption peak around 1,337 cm^{-1} was the typical vibration of the Ti-OH bond (Tan *et al.* 2011). No new bands, such as Ti-N stretch at 510 cm^{-1} (Zeng *et al.* 2016), could be observed on the composite material spectrum, which indicated that no new chemical groups were formed. From the XRD pattern and FT-IR spectra of TiO_2@ZIF-8 calcined at 300 °C, we affirmed that TiO_2 had adhered to the surface of ZIF-8.

Adsorption kinetics and isotherms of As(III)

To analyse the adsorption kinetics of As(III) by TiO_2, ZIF-8, and TiO_2@ZIF-8 in dark conditions, pseudo-first-order and pseudo-second-order models were used to describe the sorption kinetic data.

The pseudo-first-order is shown in Equation (1):

$$q_t = q_{eq}(1 - e^{-k_1 t}) \quad (1)$$

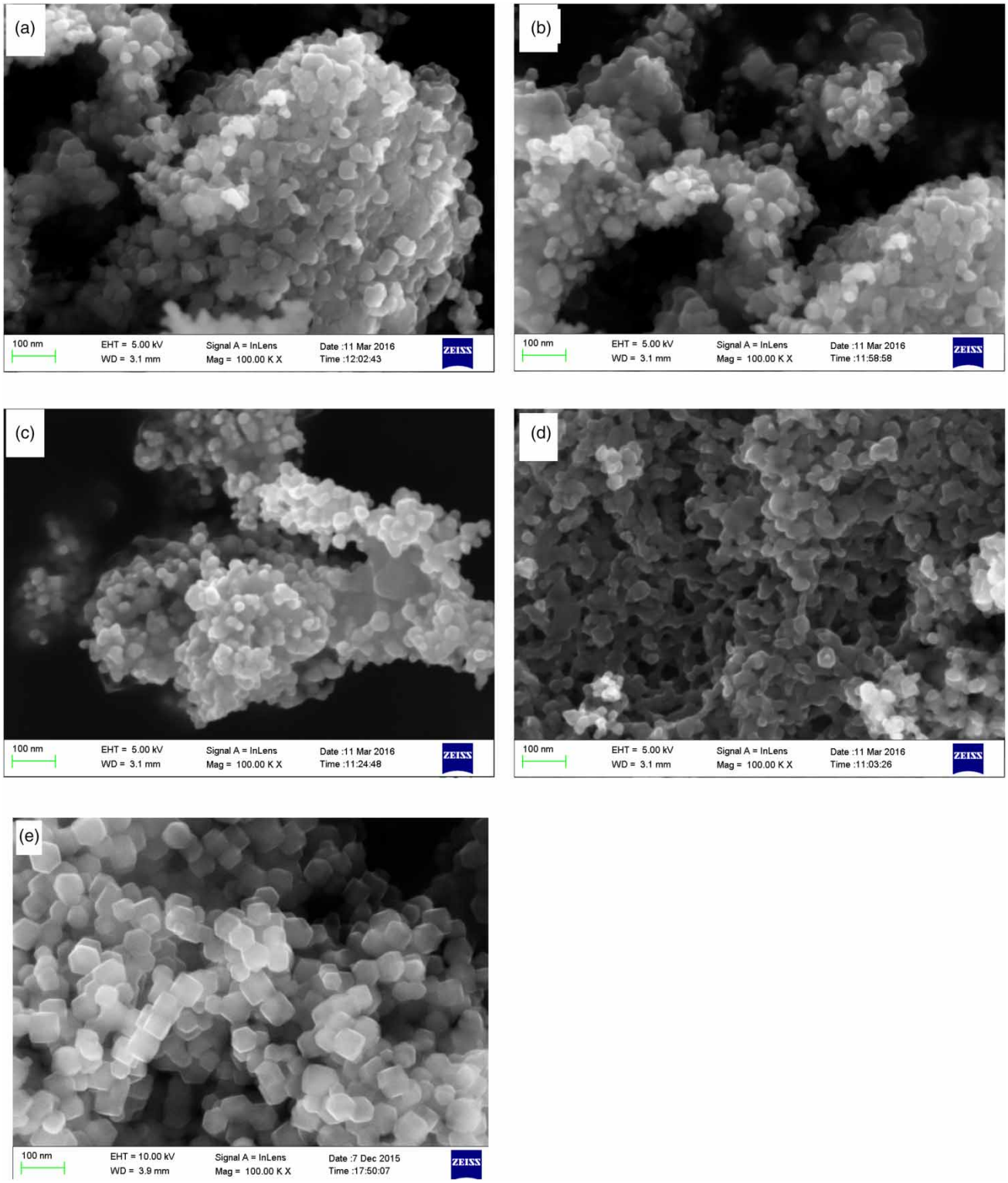

Figure 3 | SEM images for TiO_2@ZIF-8 with the different calcination temperatures: (a) 100 °C; (b) 200 °C; (c) 300 °C; (d) 400 °C; and (e) ZIF-8.

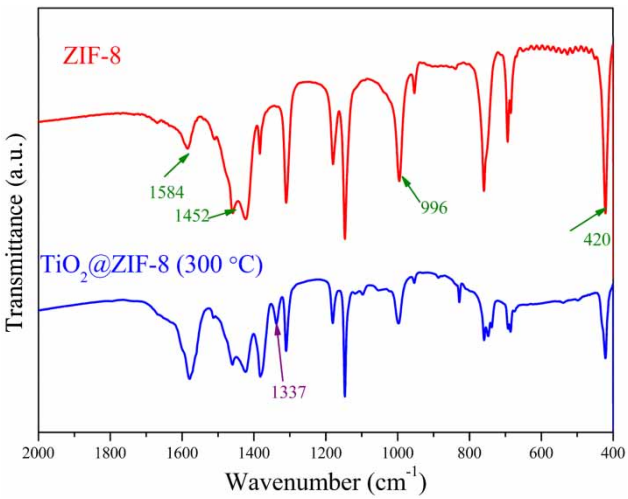

Figure 4 | FT-IR spectra of ZIF-8 and TiO_2@ZIF-8 (300 °C).

The pseudo-second-order is shown in Equation (2):

$$q_t = \frac{q_{eq}^2 k_2 t}{1 + k_2 q_{eq} t} \tag{2}$$

where q_t and q_{eq} are adsorption capacities at time t (h) and at equilibrium respectively (mmol/g), and k_1 (h^{-1}) and k_2 (g/mmol·h) are the sorption rate constants for the pseudo-first-order and pseudo-second-order models, respectively.

As shown in Figure 5, the adsorption of As(III) on TiO_2-@ZIF-8 and ZIF-8 was fast in the beginning, and then quickly levelled off, and the time required to reach the adsorption equilibrium was only 60 min. The adsorption capacity of ZIF-8 was higher than TiO_2@ZIF-8, which is because the porosity and specific surface of ZIF-8 was higher than that of TiO_2. The adsorption rate constants k_1 (see Table 1) of ZIF-8 and TiO_2@ZIF-8 were similar, and the rate of TiO_2@ZIF-8 was about 3.5 times faster than that of TiO_2.

To measure the adsorption capacities and behaviours of As(III) on TiO_2@ZIF-8 in dark conditions, the Langmuir and Freundlich isotherm models were applied to explain the adsorption equilibriums.

The Langmuir isotherm is shown in Equation (3):

$$Q_e = \frac{QK_L C_e}{1 + K_L C_e} \tag{3}$$

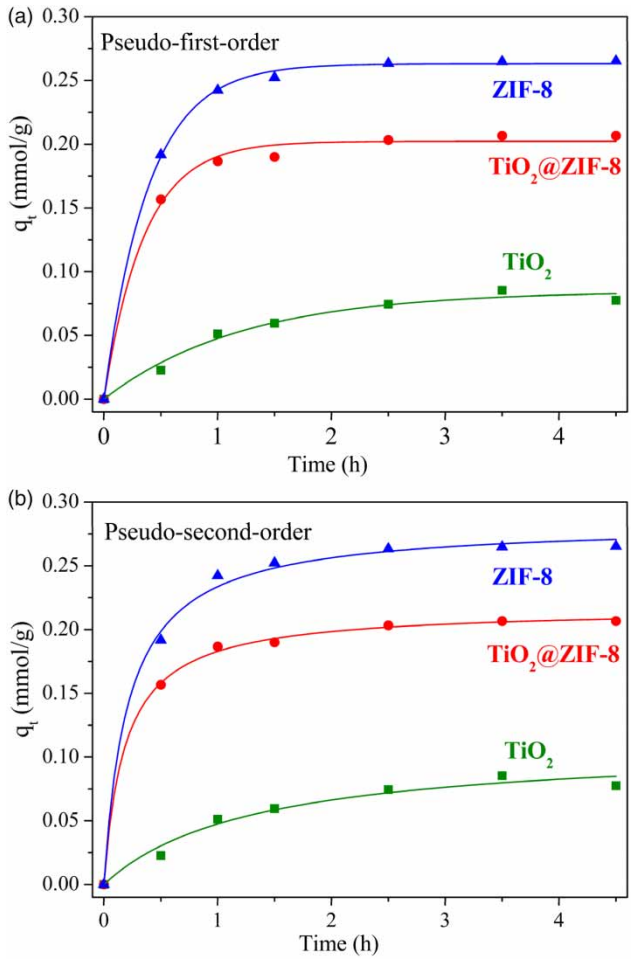

Figure 5 | Adsorption kinetics of As(III) on TiO_2, ZIF-8, and TiO_2@ZIF-8 in dark conditions: pseudo-first-order (a), pseudo-second-order (b); the initial As(III) concentration of 2 mg/L, pH 7.0, solid/solution ratio of 0.04 g/L, and T = 25 ± 1 °C.

Table 1 | Parameters of adsorption kinetics for As(III) adsorption on TiO_2, ZIF-8, and TiO_2@ZIF-8 in dark conditions

	Pseudo-first-order			Pseudo-second-order		
Material	q_{eq} (mmol/g)	k_1 (h^{-1})	R^2	q_{eq} (mmol/g)	k_2 (g/mmol·h)	R^2
TiO_2	0.0848	0.823	0.979	0.110	6.995	0.966
ZIF-8	0.263	2.565	0.998	0.284	16.467	0.996
TiO_2@ZIF-8	0.202	2.836	0.994	0.217	24.763	0.999

The Freundlich isotherm is shown in Equation (4):

$$Q_e = K_F C_e^{1/n} \tag{4}$$

where Q_e and Q are the adsorption capacity and the maximum amount respectively, mmol/g; C_e is the equilibrium concentration of As(III) (mg/L); K_L is the Langmuir equilibrium constant (L/mg); K_F is the relative adsorption capacity (mmol/g) and n is the intensity of adsorption.

The adsorption isotherms are shown in Figure 6, and the parameters are summarized in Table 2. The adsorption equilibrium data were better fitted by the Freundlich model than the Langmuir model, which means a heterogeneous sorption (Jian *et al.* 2015). The maximum adsorption capacity for As(III) from the Langmuir model was determined at 0.51 mmol/g.

Influential factors for the removal of As(III)

The effect of illumination condition was analysed in the results of UV-light ($\lambda < 400$ nm) or visible light ($\lambda > 400$ nm) irradiation (see Figure 7). The results indicated that the removal rate increased rapidly under UV-light irradiation,

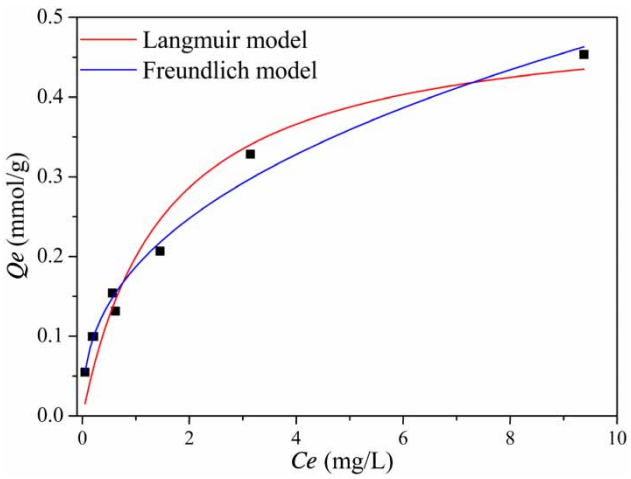

Figure 6 | Adsorption isotherms of As(III) on TiO_2@ZIF-8 in dark conditions. Initial As(III) concentration range from 0.2 to 10 mg/L, pH 7.0, solid/solution ratio of 0.04 g/L, and T = 25 ± 1 °C.

Table 2 | Parameters of adsorption isotherms for As(III) adsorption on TiO_2@ZIF-8 in dark conditions

	Langmuir model			Freundlich model		
Material	***Q* (mmol/g)**	***K*$_L$ (L/mg)**	**R^2**	***n***	***K*$_F$ (mmol/g)**	**R^2**
TiO_2@ZIF-8	0.51	0.65	0.93	2.47	0.19	0.98

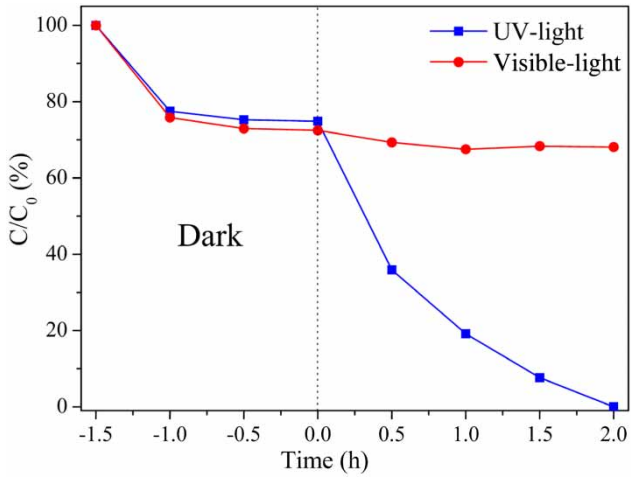

Figure 7 | Effect of illumination condition on the removal of As(III). C_0 is the initial concentration of As(III), and C is the concentration of As(III) at different reaction times. C/C_0 represents the ratio C to C_0. C_0 of 2 mg/L, pH 7.0, solid/solution ratio of 0.04 g/L.

and other species of arsenic were not found except As(III). By comparison of the amounts of As(III) removed with and without UV-light, it can be affirmed that the disappearance of As(III) is mainly caused by photocatalytic oxidation instead of only adsorption. The mechanism of the oxidation reaction catalyzed by TiO_2@ZIF-8 was proposed as the following four steps (Yao *et al.* 2010):

(1) The adsorption of As(III) on the surface of TiO_2;
(2) The oxidation of As(III) to As(V);
(3) The desorption of As(V) from the surface of TiO_2;
(4) The adsorption of As(V) on the surface of ZIF-8 or TiO_2.

In order to evaluate the effect of the removal of As(III) by TiO_2@ZIF-8, the comparative experiments with TiO_2 and ZIF-8 were carried out, and the results are shown in Figure 8. Under the UV-light irradiation, the concentrations of As(III) rapidly decreased for the pure TiO_2 and TiO_2@ZIF-8, and the concentration decreased slightly for ZIF-8, which was due to the ozone that was produced by the xenon lamp oxidizing As(III) to As(V), which was then adsorbed by ZIF-8. The more significant finding was that TiO_2@ZIF-8 was more effective for the removal of As(III) in comparison to TiO_2. The reason may be that the band gap of TiO_2 decreased, which enhanced the effect of photocatalytic oxidation (Chandra *et al.* 2015). Compared to TiO_2 and ZIF-8, almost 100% arsenic removal was achieved by TiO_2@ZIF-8,

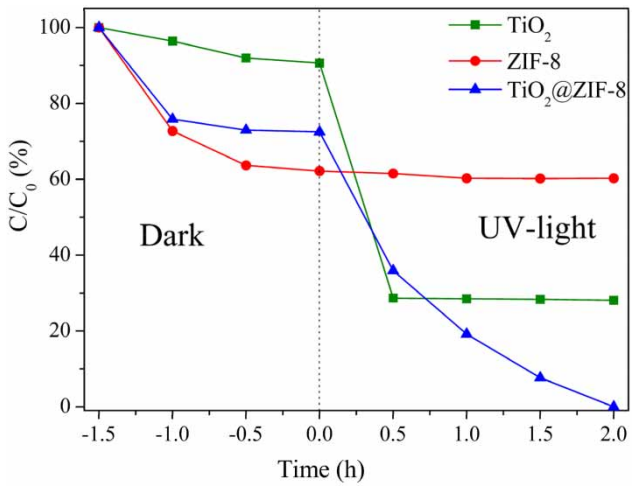

Figure 8 | Effect of As(III) removal with different materials. C_0 of 2 mg/L, pH 7.0, solid/solution ratio of 0.04 g/L.

indicating a great treatment efficiency to satisfy the WHO's drinking water standard for arsenic.

The removal of As(III) by TiO_2@ZIF-8 under UV-light irradiation was also studied at the various initial As(III) concentrations ranging from 0.5 mg/L to 10 mg/L with the solid/solution ratio of 0.04 g/L (see Figure 9). The findings indicated that the removal amount (mmol/g) of As(III) increased with the increase of the initial concentration, from 0.16 mmol/g (0.5 mg/L) to 2.7 mmol/g (10 mg/L). However, the removal rates of As(III) gradually decreased with the concentration increase. The removal rate of As(III) was 100% when the initial As(III) concentration was below 2 mg/L, and 72% when the initial concentration was 10 mg/L. The decrease in the percentage of removal rate can be explained by the fact that the active sites of TiO_2@ZIF-8 reached saturation with the increase in initial concentration. In general, TiO_2@ZIF-8 has the advantage of producing less polluted water with a low concentration of As(III), especially less than 2 mg/L.

The solution pH influences both the binding sites on the surface of the adsorbent and the distribution of arsenic species, thus it may have an impact on the removal of As(III). The effect of media pH on the removal behaviour was analysed in the pH range 4–10. (see Figure 10). The results show that the adsorption rate was similar at different pH values in dark conditions, and the removal rate was not significantly different at a pH of 4–7 under UV-light irradiation. The removal rate was 100% and 89.34%, corresponding to pH 4 and 10, respectively. So TiO_2@ZIF-8 adapts to a comparatively broad range of pH, and similar As(III) removal behavior by nanocrystalline TiO_2 was observed (Pena *et al.* 2006).

In order to assess the feasibility of reutilization of TiO_2@ZIF-8 calcined at 300 °C, it was subjected to a series of adsorption/desorption cycles (Figure 11). The results show that the removal rate of As(III) remained above 90% after the TiO_2@ZIF-8 had been used for five times. Thus, it is suggested that the deposited TiO_2 particles had firmly attached to the surface of ZIF-8, and cannot be easily

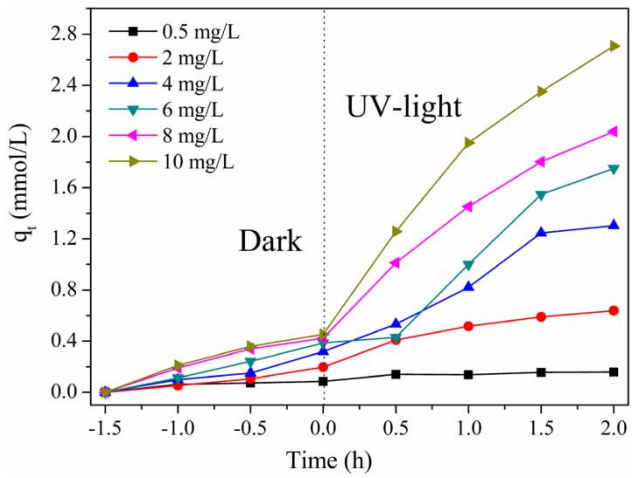

Figure 9 | Effect of the different initial concentrations on the removal of As(III). pH 7.0, solid/solution ratio of 0.04 g/L.

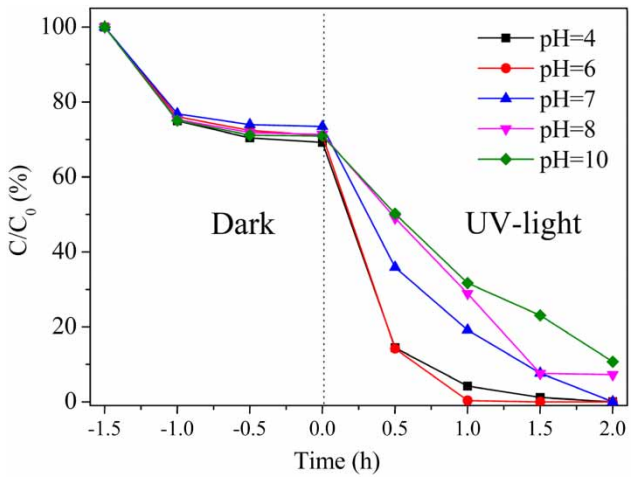

Figure 10 | Effect of As(III) removal in samples under different pH conditions. C_0 of 2 mg/L, solid/solution ratio of 0.04 g/L.

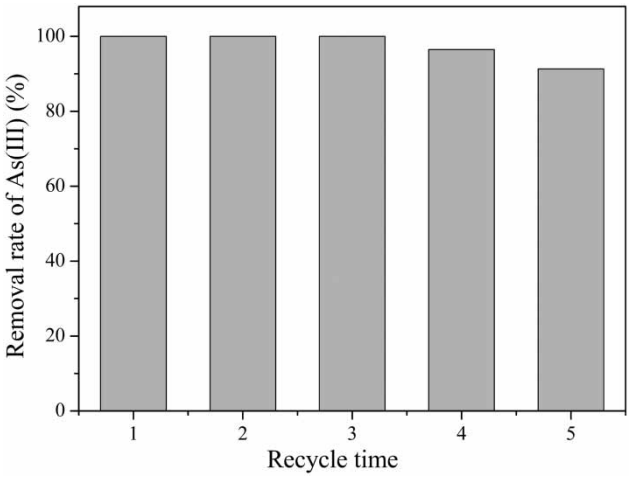

Figure 11 | Influence of reutilization cycles for the removal rate of As(III).

exfoliated from the ZIF-8 with mechanically stirred solutions for a long period.

CONCLUSIONS

The optimum synthesis condition of TiO_2@ZIF-8 was calcination at 300 °C for 3 h by the sol-gel method. In contrast with the single ZIF-8 or TiO_2, TiO_2@ZIF-8 had a better removal ability to deal with a low concentration of As(III), especially less than 2 mg/L, under UV-light irradiation. This material could adapt to a wide pH range, and the removal rate was up to 100% in the pH range from 4 to 7. In addition, the composite material can be used repeatedly and the high removal properties were maintained with a slight decline. Through the above analysis and discussion, we propose that TiO_2@ZIF-8 is a good prospect for the removal of As(III) from water containing low initial As(III) concentrations.

REFERENCES

Bang, S., Patel, M., Lippincott, L. & Meng, X. G. 2005 Removal of arsenic from groundwater by granular titanium dioxide adsorbent. *Chemosphere* **60** (3), 389–397.

Bissen, M., Vieillard-Baron, M. M., Schindelin, A. J. & Frimmel, F. H. 2001 TiO_2-catalyzed photooxidation of arsenite to arsenate in aqueous samples. *Chemosphere* **44** (4), 751–757.

Chandra, R., Mukhopadhyay, S. & Nath, M. 2015 TiO_2@ZIF-8: a novel approach of modifying micro-environment for enhanced photo-catalytic dye degradation and high usability of TiO_2 nanoparticles. *Materials Letters* **164**, 571–574.

Guan, X. H., Du, J. S., Meng, X. G., Sun, Y. K., Sun, B. & Hu, Q. H. 2012 Application of titanium dioxide in arsenic removal from water: a review. *Journal of Hazardous Materials* **215**, 1–16.

Hu, Y., Kazemian, H., Rohani, S., Huang, Y. N. & Song, Y. 2011 In situ high pressure study of ZIF-8 by FTIR spectroscopy. *Chemical Communications* **47** (47), 12694–12696.

Jian, M. P., Liu, B., Zhang, G. S., Liu, R. P. & Zhang, X. W. 2015 Adsorptive removal of arsenic from aqueous solution by zeolitic imidazolate framework-8 (ZIF-8) nanoparticles. *Colloids and Surfaces A-Physicochemical and Engineering Aspects* **465**, 67–76.

Lan, J. 2015 Removal of arsenic from aqueous systems by use of magnetic Fe_3O_4@TiO_2 nanoparticles. *Research on Chemical Intermediates* **41** (6), 3531–3541.

Liu, H., Zuo, K. C. & Vecitis, C. D. 2014 Titanium dioxide-coated carbon nanotube network filter for rapid and effective arsenic sorption. *Environmental Science & Technology* **48** (23), 13871–13879.

Liu, B., Jian, M. P., Liu, R. P., Yao, J. F. & Zhang, X. W. 2015 Highly efficient removal of arsenic(III) from aqueous solution by zeolitic imidazolate frameworks with different morphology. *Colloids and Surfaces A-Physicochemical and Engineering Aspects* **481**, 358–366.

Mazumder, D. N. G., Haque, R., Ghosh, N., De, B. K., Santra, A., Chakraborty, D. & Smith, A. H. 1998 Arsenic levels in drinking water and the prevalence of skin lesions in West Bengal, India. *International Journal of Epidemiology* **27** (5), 871–877.

Miller, S. M. & Zimmerman, J. B. 2010 Novel, bio-based, photoactive arsenic sorbent: TiO_2-impregnated chitosan bead. *Water Research* **44** (19), 5722–5729.

Mohan, D. & Pittman, C. U. 2007 Arsenic removal from water/wastewater using adsorbents – a critical review. *Journal of Hazardous Materials* **142** (1–2), 1–53.

Pena, M. E., Korfiatis, G. P., Patel, M., Lippincott, L. & Meng, X. G. 2006 Adsorption of As(V) and As(III) by nanocrystalline titanium dioxide. *Water Research* **39** (11), 2327–2337.

Pirila, M., Martikainen, M., Ainassaari, K., Kuokkanen, T. & Keiski, R. L. 2011 Removal of aqueous As(III) and As(V) by hydrous titanium dioxide. *Journal of Colloid and Interface Science* **353** (1), 257–262.

Qu, J. H. 2008 Research progress of novel adsorption processes in water purification: a review. *Journal of Environmental Sciences (China)* **20** (1), 1–13.

Tan, J., Yang, L. X., Kang, Q. & Cai, Q. Y. 2011 In situ ATR-FTIR and UV-visible spectroscopy study of photocatalytic oxidation of ethanol over TiO_2 nanotubes. *Analytical Letters* **44** (6), 1114–1125.

Tran, U. P. N., Le, K. K. A. & Phan, N. T. S. 2011 Expanding applications of metal-organic frameworks: zeolite imidazolate framework ZIF-8 as an efficient heterogeneous catalyst for the knoevenagel reaction. *ACS Catalysis* **1** (2), 120–127.

Wei, Z. G., Liang, K., Wu, Y., Zou, Y. D., Zuo, J. H., Arriagada, D. C., Pan, Z. C. & Hu, G. H. 2016 The effect of pH on the adsorption of arsenic(III) and arsenic(V) at the TiO_2 anatase [101] surface. *Journal of Colloid and Interface Science* **562**, 252–259.

Yao, S. H., Jia, Y. F., Shi, Z. L. & Zhao, S. 2010 Photocatalytic oxidation of arsenite by a composite of titanium dioxide and activated carbon fiber. *Photochemistry and Photobiology* **86** (6), 1215–1221.

Yu, B., Wang, F. F., Dong, W. B., Hou, J., Lu, P. C. & Gong, J. B. 2015 Self-template synthesis of core-shell ZnO@ZIF-8 nanospheres and the photocatalysis under UV irradiation. *Materials Letters* **156**, 50–53.

Zeng, X., Huang, L., Wang, C., Wang, J. S., Li, J. T. & Luo, X. T. 2016 Sonocrystallization of ZIF-8 on electrostatic spinning TiO_2 nanofibers surface with enhanced photocatalysis property through synergistic effect. *ACS Applied Materials & Interfaces* **8** (31), 20274–20282.

Zhang, L. K., Qin, X. Q., Tang, J. S., Liu, W. & Yang, H. 2017 Review of arsenic geochemical characteristics and its significance on arsenic pollution studies in karst groundwater, Southwest China. *Applied Geochemistry* **77**, 80–88.

Zhu, M. Q., Venna, S. R., Jasinski, J. B. & Carreon, M. A. 2011 Room-temperature synthesis of ZIF-8: the coexistence of ZnO nanoneedles. *Chemistry of Materials* **23** (16), 3590–3592.

First received 5 January 2017; accepted in revised form 21 April 2017. Available online 9 May 2017